Mineralium Deposita (2001) 36: 149–164

ARTICLE

Evandro Luiz Klein · Reginaldo Alves dos Santos
Kazuo Fuzikawa · Rômulo Simões Angélica

Hydrothermal fluid evolution and structural control of the Guarim gold mineralisation, Tapajós Province, Amazonian Craton, Brazil

Received: 3 March 2000 / Accepted: 21 October 2000

Abstract Fluid inclusion and structural studies were carried out at the Guarim gold deposit in the Palaeoproterozoic Tapajós province of the Amazonian craton. Guarim is a fault-hosted gold deposit cutting basement granitoids. It consists of a quartz vein, which is massive in its inner portions, grading laterally either to a massive or to cavity-bearing quartz vein associated with hydrothermal breccias. The wallrock alteration comprises chlorite, carbonate, white mica and sulphide minerals, with free gold occurring within quartz grains and spatially associated with sulphide mineral grains. Petrographic, microthermometric and Laser Raman investigations recognised CO_2-rich, mixed H_2O–CO_2, and H_2O fluid inclusions. The coexisting CO_2 and H_2O–CO_2 inclusions were interpreted as primary immiscible fluids that formed the gold-bearing vein. The H_2O inclusions were considered a product of later infiltration of fluids unrelated to the mineralising episode. The mineralising fluid has CO_2 ranging typically from 5–10 mol%, contains traces of N_2, has salinities of ~5 wt% NaCl equiv., and densities varying between 0.85 and 0.95 g/cm^3. The P–T estimations bracket gold deposition between 270–320 °C and 0.86–2.9 kb; f_{O_2}–f_{S_2}–pH estimates suggest a reduced, near-neutral character for the fluid. Variations in the physico-chemical properties, as demonstrated by the fluid inclusion study, resulted from a combination of fluid immiscibility and pressure fluctuation. This interpretation, combined with textural and structural evidence, suggests the emplacement of the mineralised vein in an active fault and at a rather shallow level (4–7 km). The geological and structural setting, deposit-scale textures and structures, wallrock alteration and physico-chemical fluid properties are compatible with those of epizonal to mesozonal orogenic lode gold deposits.

Editorial handling: L. Diamond

E. L. Klein (✉)
CPRM/Geological Survey of Brazil, Av. Dr. Freitas,
3645, Belém-PA, CEP: 66095-110, Brazil
e-mail: eklein@amazon.com.br
Tel.: +55-91-2768577; Fax: +55-91-2764020

R. Alves dos Santos
CPRM/Geological Survey of Brazil,
Av. Ulysses Guimarães, 2862,
Centro Administrativo da Bahia, Salvador-BA,
CEP: 41213-000, Brazil

K. Fuzikawa
CDTN/CNEN (National Committee of Nuclear Energy) –
Rua Mario Werneck, s/n, Pampulha, Belo Horizonte-MG,
CEP: 30270-010, Brazil

R. Simões Angélica
UFPA (Federal University of Pará) – C.P. 1611,
Belém-PA, CEP: 66075-110, Brazil

Introduction

The Palaeoproterozoic Tapajós gold province (Faraco et al. 1997) of the Amazonian craton has been a major alluvial and supergene gold producer since 1958 (600 t, unofficial data), worked exclusively by poorly mechanised small miners (the so-called *garimpeiros*). This activity has led to the discovery of >100 small primary gold deposits in several camps and small districts in the province, drawing the attention of many major and junior companies. Given the importance of this province, CPRM (Geological Survey of Brazil) started a regional mapping and geophysical programme in 1996 and comprehensive petrological, geochemical and geochronological studies have been undertaken to enhance the knowledge of the geological evolution of this province. Also, efforts have been made to better understand Tapajós gold metallogeny. A series of contributions describing the main characteristics of the mineralisation (Faraco et al. 1997; Almeida et al. 1998; Costa and Carvalho 1999; Klein et al. 1999) and structural controls (Santos 1998, 1999), as well as to establish possible genetic models (Coutinho et al. 1997; Dreher et al. 1998) were completed, but they mostly are restricted to internal reports and to contributions for Brazilian meetings.

Among various gold camps and smaller districts, the historically important Cuiú-Cuiú gold camp in the Tapajós province hosts several alluvial, supergene and hypogene gold deposits. The latter include gold–quartz vein deposits (Guarim, Jerimum de Baixo, Jerimum de Cima, Raimundinha), and less abundant stockworks (Nhô, Carneirinho), as well as several undeveloped showings. Geophysical surveys, soil geochemistry and drilling have been undertaken at these prospects by mining companies. The results (gold grades and resources) are not available, but the prospects are presently subeconomic as large targets. However, small mining operations have extracted, through manual workings, 1–1.5 kg of free-milling gold per month from some prospects.

As a contribution for a further understanding of the Tapajós province metallogeny, this paper presents constraints on the hydrothermal fluid characteristics of the Guarim gold prospect. This well-exposed prospect is representative of an important and widespread style of mineralisation in the province, and detailed petrographic, fluid inclusion and structural studies provide interesting information on textures, host structures, depth of vein formation and ore-fluid chemistry and systematics for a typical quartz vein deposit in the Cuiú-Cuiú camp.

Analytical procedures

Microthermometric measurements were carried out on fluid inclusions in two doubly-polished sections from two samples, one collected at the centre and one at the margin of the gold-bearing vein quartz (see vein description below). Work was done using a Chaixmeca heating and freezing stage at the Pará Federal University (UFPA), in Belém, Brazil, following the procedures outlined by Roedder (1984) and Shepherd et al. (1985). Calibration has been done with available standards. The estimated precision of the measurements is ± 0.5 °C for temperatures lower than −20 °C; ± 0.3 °C for the interval −20 to 40 °C; and ± 5 °C for temperatures >40 °C.

Selected fluid inclusions were analysed by a laser-excited Dilor multichannel microprobe at the Laboratory of Optics of the Minas Gerais Federal University (UFMG), in Belo Horizonte, Brazil, using the 514.53-nm line of an argon laser (green light). Integration time was 10 s with 10 accumulations for each spectral line. Instrumental settings were kept constant during the analyses.

X-ray diffraction (XRD) analyses (powder method) from the total samples and selected minerals were carried out on a Phillips PW 3710 diffractometer at UFPA with the following standard conditions: CuKα1 radiation (1.54050 A), 45 kV, 40 mA, graphite monocromator and 2θ varying from 5–65°, in steps of 0.02°. The results (diffractograms) were evaluated through the Phillips-APD software.

Geological setting

The Tapajós gold province forms the central part of the Amazonian craton (Fig. 1). This major craton has been previously interpreted to have formed by the amalgamation of Archaean crustal fragments along Proterozoic mobile belts and/or by generation of new crust in magmatic arc environments (Cordani and Brito Neves 1982; Teixeira et al. 1989). More recently, supported by a considerable amount of geochronological data, the Amazonian craton was divided into several tectonic-geochronological domains representing crustal fragments, mobile belts and magmatic arcs that eventually formed the large craton at the end of the Mesoproterozoic (Tassinari et al. 1996; Cordani and Sato 1999; Tassinari and Macambira 1999; Santos et al. 2000). The Tapajós gold province is included within the Ventuari–Tapajós domain of Tassinari and Macambira (1999) or the Tapajós–Parima province of Santos et al. (2000).

The geological knowledge of the Tapajós area is mainly derived from the regional mapping programme of CPRM (Almeida et al. 2000; Bahia and Quadros 2000; Ferreira et al. 2000; Klein and Vasquez 2000; Vasquez and Klein 2000), in which two tectonic domains were defined (Klein and Vasquez 2000). There is an orogenic domain, mainly affected by compressive/transpressive tectonics, and a post-orogenic to anorogenic domain, mainly extensional. Calc-alkaline grey gneisses with minor migmatites and metagranitoids of the Cuiú-Cuiú Complex are the oldest rocks (2033 Ma) in the province. This complex occurs in close association with the broadly coeval metasedimentary rock succession of the Jacareacanga Group. Both units are interpreted as related to early stages of magmatic arc development (Almeida et al. 1999). The youngest rocks in the orogenic domain are the syn- to late-orogenic, medium- to high-K metagranitoids of the Creporizão Intrusive Suite, which intruded the basement rocks between 1990 and 1960 Ma (Ricci et al. 1999; Klein and Vasquez 2000; Santos et al. 2000). The subsequent post-orogenic to anorogenic domain includes calc-alkaline granitoids of the Parauari Intrusive Suite (1900–1890 Ma) and alkaline, high-K granitoids and felsic to intermediate volcanics of the Maloquinha Intrusive Suite and Iriri Group (1890–1880 Ma) respectively (Klein et al. 1999; Vasquez et al. 1999). A series of intermediate to dominantly mafic intrusions, a few hosting gold mineralisation (Quadros et al. 1999), as well as anorogenic granitoids, lamprophyres and sedimentary cover, completes the Palaeoproterozoic stratigraphy of the Tapajós province.

The province was affected by an older deformational event attributed to a subduction-related oblique collisional event (Almeida et al. 1999). It is represented by the NNE–SSW-oriented banding of the Cuiú-Cuiú gneisses and by some thrust faults, which were responsible for placing these gneisses in contact with the supracrustal rocks of the Jacareacanga Group.

A later, second deformational event comprises major NNW–SSE-trending curvilinear to sigmoidal lineaments, tens to a few hundreds of kilometres long (Fig. 1). These lineaments represent continuous to discontinuous brittle faults and subordinate brittle–ductile and ductile shear zones developed essentially under a dominantly sinistral strike–slip regime (Santos 1999). These structures have played a major role in outlining the shape and the geometry of the lithostratigraphic units, controlling the emplacement of several generations of granitoids and mafic rocks, and establishing sedimentary basins (Klein et al. 1997; Santos 1999). The strike–slip system is interpreted as a progressive and episodic deformational event related to the E–W to ENE–WSW compressive stress ($\sigma 1$), as shown by geometric relationships of minor subsidiary structures.

Gold mineralisation in the Tapajós province is strongly related to this NNW–SSE strike–slip system, and most of the deposits are located close to the major lineaments. Camp scale and deposit scale structural data show that most of the deposits are positioned in subvertical structures (fault-fill veins, shear veins), which are geometrical and genetically linked to the major lineaments. Gold-hosting structures are dilatational sites represented by extensional fractures, dilatational jogs, horse-tail terminations, intersection of faults and fractures with other structures (dykes, lithological contacts) and zones of intense fracturing (Klein et al. 1999; Santos 1999).

Geology and structural aspects of the Cuiú-Cuiú gold camp

The Cuiú-Cuiú gold camp (Figs. 1 and 2) is dominated by the Cuiú-Cuiú Complex, which comprises mainly granitoids, metagranitoids (quartz diorites to tonalites

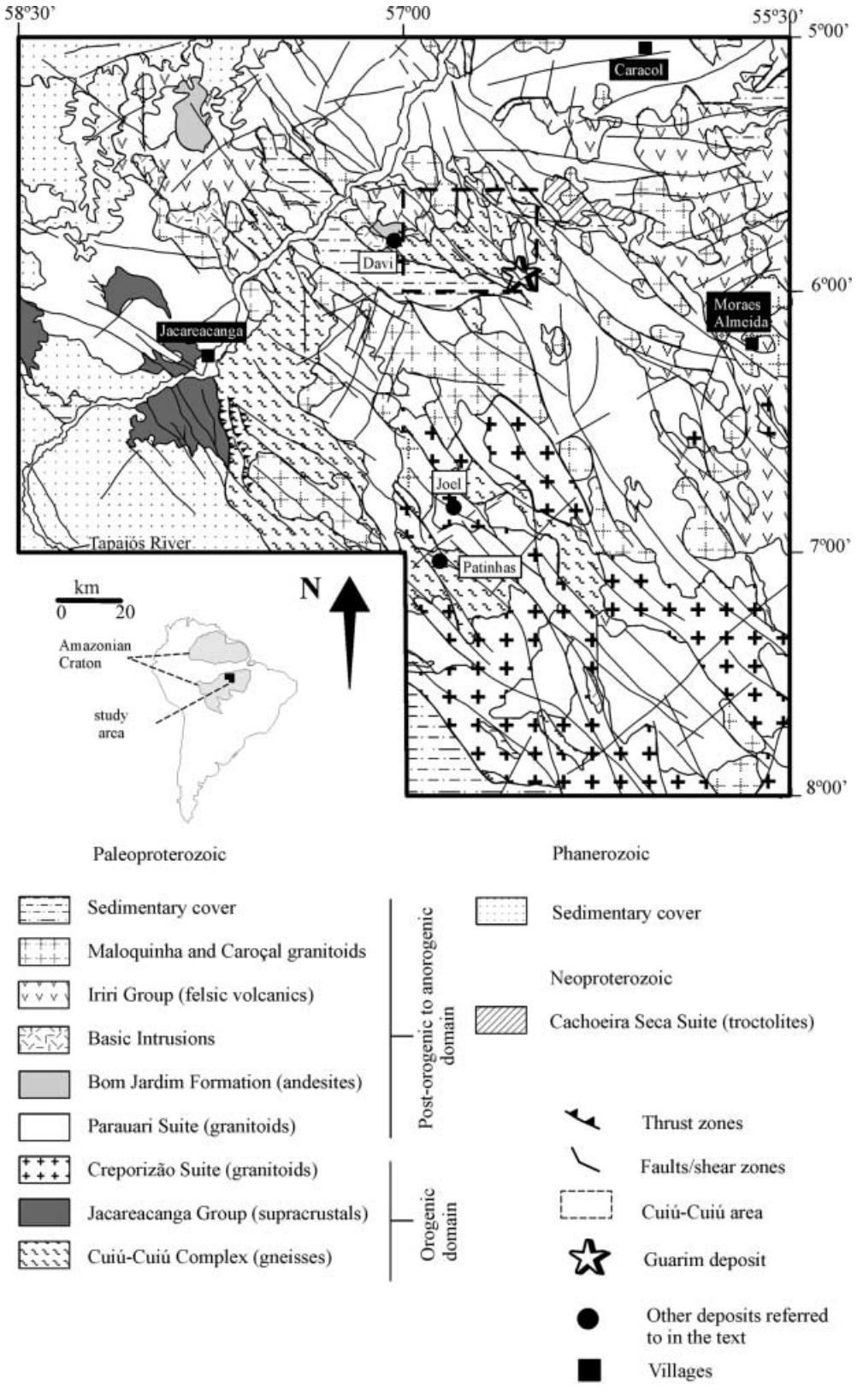

Fig. 1 Geological map of the Tapajós gold province (after Almeida et al. 2000; Bahia and Quadros 2000; Ferreira et al. 2000; Klein and Vasquez 2000; Vasquez and Klein 2000)

and granodiorites, with subordinate monzogranites) and minor gneissic rocks (Bahia and Quadros 2000). They are medium- to coarse-grained, porphyritic to locally equigranular rocks, but also display a steeply-dipping, mylonitic and/or magmatic foliation, trending to N20°E. A series of E–W-trending diabase dykes and N–S-trending aplitic veins cut these rocks and are also locally deformed. The gneisses are coarse-grained with a

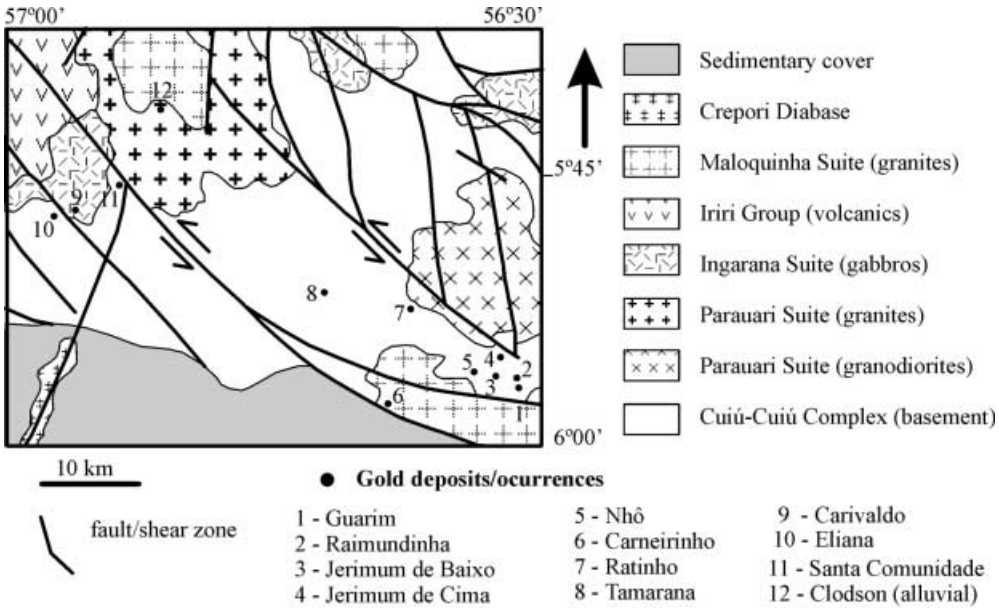

Fig. 2 Geological map of the Cuiú-Cuiú area, with the location of gold deposits (modified from Bahia and Quadros 2000)

dominantly granodioritic composition, and their foliation parallels the foliation of the granitoids. The metamorphism that affected the Cuiú-Cuiú rocks reached medium, to locally high, amphibolite facies conditions. Calc-alkaline granitoids of the Parauari Intrusive Suite intrude the Cuiú-Cuiú rocks, and include predominantly medium-grained porphyritic monzogranites and granodiorites. The Parauari Suite rocks exhibit well-preserved igneous features and are only locally deformed along discrete shear zones (Bahia and Quadros 2000). The southern part of the Cuiú-Cuiú Complex is defined by a narrow E–W to NNW–SSE-trending basin, filled with the sedimentary rocks of the Proterozoic Buiuçu Formation.

The rocks of the Cuiú-Cuiú area and their associated gold mineralisation are broadly bounded by two major NNW–SSE sinistral faults (Figs. 1 and 2), which are part of the regional strike–slip system. Different styles of mineralisation have been recognised (Santos 1998), such as stockworks, breccias and veins. The veins are located dominantly in both sinistral and dextral NE–SW and NW–SE faults, and locally along transpressional sites of the major faults, such as in positive flower structures. Additionally, gold–quartz veinlets occur as oblique tension gashes and small extensional zones (pull-apart).

Local structure, vein textures and wallrock alteration

Mineralisation and hydrothermal alteration at the Guarim gold deposit are closely associated with a quartz vein confined to a steeply-dipping (75°) strike–slip fault trending N75°E. This fault traverses a weakly-foliated, coarse-grained porphyritic rock of granodiorite to quartz–diorite composition, attributed to the Cuiú-Cuiú Complex. Thin, subvertical oblique extensional veinlets also occur adjacent to the vein (Fig. 3). Dislocation at the interface between vein and host rock has produced a well-defined slip plane containing subhorizontal slickenlines. These slickenlines, together with the orientation of the extensional veinlets, indicate a sinistral movement.

The vein varies from 0.4–0.7 m in thickness. Its length and vertical extent are unknown, but it could be traced for 200 m along-strike to the north. It is surrounded by asymmetrical alteration zones as wide as 4 m (Fig. 3). These have been better developed in the hanging wall of the fault. The inner alteration zone here comprises a network of millimetre- to centimetre-wide quartz veinlets and hydrothermal breccias, and grades outwards to sericite–chlorite and K-feldspar zones and then into unaltered host rock. In the footwall of the fault, alteration is poorly developed. A ductile foliation, only a few centimetres wide, has developed in the host rock (Fig. 4A) adjacent to the quartz vein (Fig. 3).

The centre of the vein is composed dominantly of milky-white, massive quartz (Fig. 4B) and minor sulphide minerals. Quartz grains are anhedral to subhedral and euhedral (hexagonal), exhibiting variable grain size and no preferential orientation. This arrangement falls into the buck texture category of Dowling and Morrison (1989) and Vearncombe (1993), which is characterised by the non-directional face-control of the tightly packed growing crystals. Undulose extinction is weak to moderate, intra- and transgranular small fractures cut the crystals and no other evidence of deformation, such as recrystallisation, was observed.

The massive central portion of the vein grades laterally to a more localised dark green to greyish portion (Fig. 4B) showing massive to open-space filling textures and significant amounts of chlorite, carbonate, white mica, sulphides and rare zircons, which compose as

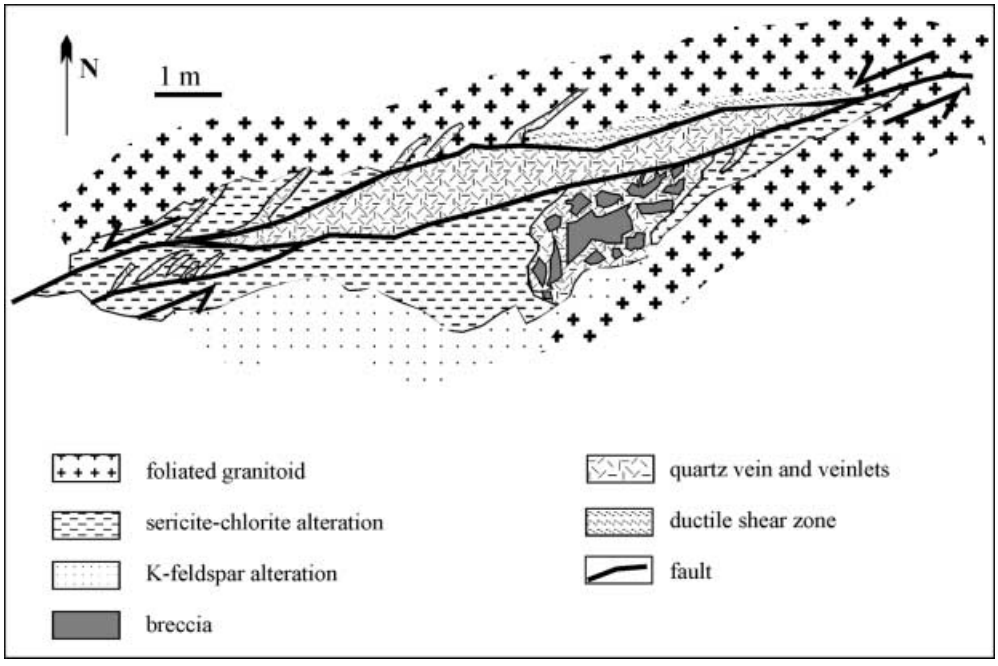

Fig. 3 Sketch map of the exposed part of the Guarim gold–quartz vein and surrounding hydrothermal alteration

much as 40 vol% of the vein. This hydrothermal mineralogy occurs either as a fine-grained matrix or as larger grains (except the carbonate, which is restricted to the groundmass) along with quartz. An XRD analysis identified calcite as the main carbonate species, whereas chlorite is represented by the chamosite polytype. Quartz grains are dominantly euhedral and smaller than in the central portion of the vein, showing no signs of deformation. Euhedral quartz is the dominant cavity-filling mineral. Subordinately, sulphide minerals and fibrous chlorite also fill the open spaces. The quartz exhibits a comb texture, which is defined by face-controlled quartz crystal growth along the C-crystallographic axis (Cox and Etheridge 1983; Dowling and Morrison 1989; Vearncombe 1993) with variable orientation of crystals.

Hydrothermal breccias occur either surrounding the vein or within the zones of extensional veinlet structures (Fig. 4C). They consist of angular fragments of the vein quartz set in a hydrothermal matrix composed of chlorite, white mica, carbonate, quartz and sulphide minerals (dominantly pyrite, with minor chalcopyrite). Hydrofracturing (Jébrak 1997) is the likely process that led to the formation of the breccias, and was triggered by variations in the fluid pressure (see discussion later) relative to the regional stress (Jébrak 1997).

Ore microscopy revealed the dominant presence of pyrite in the gold-bearing vein, occurring as well-developed crystals that are little fractured and devoid of any ductile deformation. Magnetite is very subordinate, occurring as anhedral and limpid grains, both isolated and in plane contact with pyrite, suggesting equilibrium between these minerals (Fig. 4D). Several small (< 0.05 mm) gold particles were recognised, included in quartz, but spatially associated with pyrite (Fig. 4E). Chalcopyrite was locally observed overgrowing the pyrite grains and was also detected by XRD.

Fluid inclusion study

Fluid inclusion types and distribution

About 300 fluid inclusions in two samples of the vein were microthermometrically investigated in this study. Based on their relative phase proportions at and below room temperature, and phase changes during freezing runs, three compositional types of fluid inclusions have been identified. All the three types show similar modes of occurrence in the two investigated samples and will be discussed together.

Type 1 are carbonic inclusions that, at room temperature, are either monophase or, dominantly, two-phase ($CO_{2liq} + CO_{2gas}$). They are clear to dark in appearance, with diameters varying between 5 and 15 μm, and are the least frequent of the three types. Their forms vary from irregular to ellipsoidal and negative crystal shape. Some of these inclusions may also contain a small amount of H_2O ($< 10\%$), which is petrographically and microthermometrically undetected. This assumption is based on the presence of thin rims of H_2O coating the inclusion walls that could be observed in larger inclusions.

Type 2 are H_2O–CO_2 liquid inclusions and are the predominant type with diameters ranging from 5–17 μm. They display two (H_2O_{liq}–CO_{2liq}) or three-phases (H_2O_{liq}–CO_{2liq}–CO_{2gas}) at room temperature, with optically estimated volumetric proportions of the CO_2-rich phase (VCO_2) varying from 15–50%, although clustering between 25 and 35%. The CO_2 bubble is

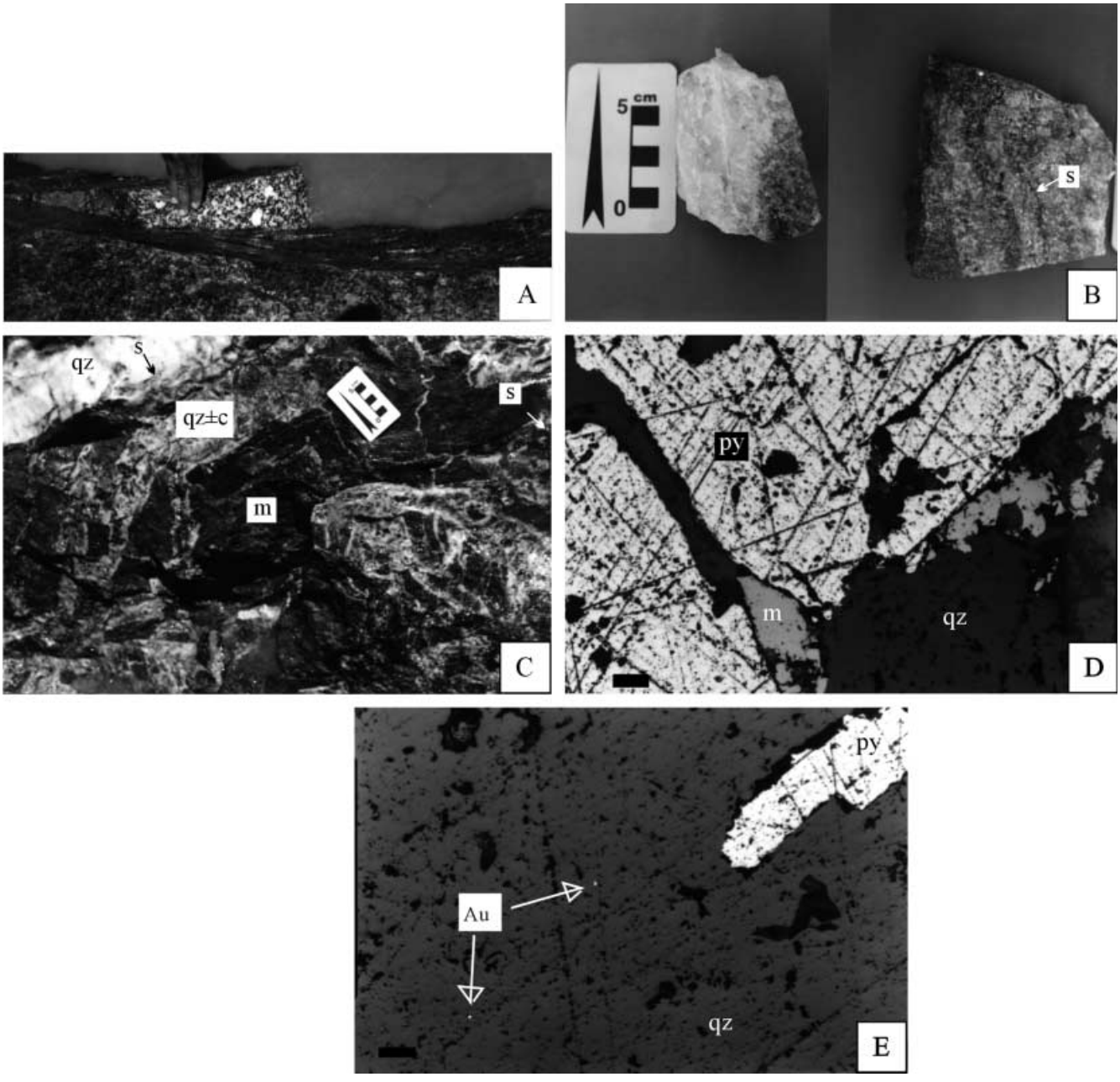

Fig. 4 Photographs showing mesoscopic and microscopic features of the Guarim deposit: **A** ductile fabric in the host metagranitoid; **B** aspects of the mineralised vein: central massive portion (*left*) and lateral, sulphidised (*S*), cavity-bearing portion (*right*) with broadly alternating quartz-rich bands (*grey*) and bands rich in white mica, carbonate and chlorite (*darker bands*); **C** hydrothermal breccias composed of white, massive quartz (*qz*), veinlets of quartz ± carbonate ($qz \pm c$), a matrix (*m*) rich in white mica, chlorite and carbonate, and sulphides (s) filling fractures; **D** reflected light photomicrograph showing the occurrence of pyrite (*py*) in the quartz (*qz*) vein and the growing of magnetite (*m*) in the margins and fractures of pyrite; **E** reflected light photomicrograph showing gold particles (*Au*) in association with pyrite (*py*), occurring in quartz (*qz*). *Scale bars* on the photomicrographs: 0.2 mm

frequently dark and the gaseous CO_2 in the three-phase inclusions is generally voluminous, almost corresponding to the total VCO_2, which makes the observation of some phase changes difficult. They exhibit more variable forms, from irregular to ellipsoidal and polygonal, negative crystal and drop-shaped.

Type 3 represents two-phase aqueous (H_2O_{liq} + H_2O_{vap}) fluid inclusions, having characteristic clear appearance with diameters ranging typically from 6–8 μm and shapes varying from irregular to ellipsoidal and negative crystal. Filling degrees are rather constant, at ~0.95.

Most of type 1 and 2 fluid inclusions are coexistent within randomly distributed groups (Fig. 5), or occur along three-dimensional arrays, clusters and fractures confined to individual quartz grains, whereas type 3 inclusions are preferentially found in transgranular trails, although some are isolated. All three types lack any daughter minerals.

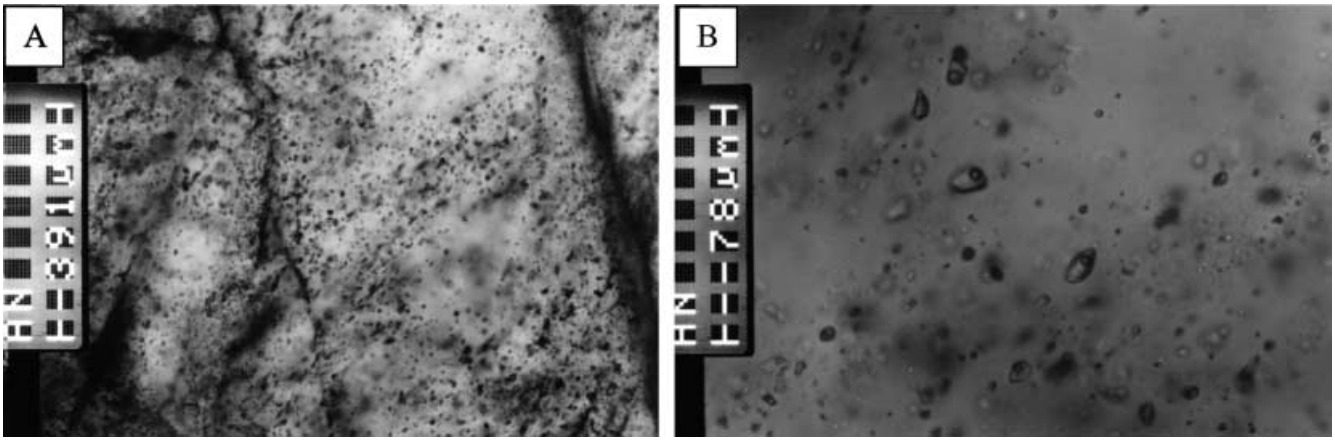

Fig. 5 Photomicrographs showing A the random distribution of the CO_2 and H_2O–CO_2 fluid inclusions cut by late trails of aqueous inclusions, and **B** the coexistence of CO_2 and H_2O–CO_2 inclusions with varying filling degrees in quartz from the Guarim deposit

Microthermometry and laser Raman spectroscopy

The CO_2-bearing inclusions (type 1) and the H_2O–CO_2 inclusions (type 2) show a similar range of CO_2 melting temperatures ($TmCO_2$), varying between −56.6 °C, the triple point of pure CO_2, and −60.7 °C, and clustering between −56.6 and −58.0 °C (Fig. 6A). This indicates the predominance of CO_2 and the presence of other volatile phases in the carbonic phase of these inclusions. Qualitative laser Raman spectroscopy performed on 13 selected type 1 and 2 fluid inclusions confirmed the dominance of CO_2 and detected N_2 as the additional volatile phase (Table 1). Also, CH_4 and H_2S were not detected within the detection limits of the technique.

The partial homogenisation of CO_2 ($ThCO_2$) of the two CO_2-bearing inclusion types occurs either to liquid or to vapour, or through the fading of the meniscus (critical homogenisation). The last two modes of homogenisation, together with the already cited high volume of the gaseous CO_2, have hampered the observation of this phase change. The inclusions homogenise between 15 and 31.1 °C (one value at 5 °C); however, most of the $ThCO_2$ measurements were recorded close to the critical point of CO_2 (31.10 °C; Fig. 6B).

In type 2 inclusions, clathrate-melting temperatures (Tmcla) always occur below $ThCO_2$, clustering between 6 and 8 °C, corresponding to salinities of between 7.5 and 3.9 wt% NaCl equiv. A few inclusions showed Tmcla as low as −5 °C, which corresponds to higher salinities (19 wt% NaCl equiv.; Fig. 6C). These inclusions are petrographically identical to the low-salinity inclusions. However, it is noteworthy that they occur in the same cluster in which high-salinity aqueous (type 3) inclusions occur.

The total homogenisation of the CO_2 phase and the H_2O phase (Tht), mostly into the liquid state, occurs over a wide temperature range, between 215 and 380 °C, but clusters between 240 and 310 °C (Fig. 6D), a range that broadly corresponds to one standard deviation (250–318 °C). The final homogenisation (to vapour) of CO_2-rich inclusions could only be observed in a few inclusions, owing to optical difficulties and to decrepitation prior to homogenisation. These inclusions homogenised (or decrepitated) between 215 and 340 °C, an almost identical range to the water-rich (type 2) inclusions.

The aqueous inclusions (type 3) show final melting temperature of ice (Tmice) ranging from −0.10 to −21.00 °C, clustering strongly between −2 and −5 °C (Fig. 6E), and corresponding to salinities of between 3.4 and 7.8 wt% NaCl equiv. The temperature of first melting of ice (eutectic temperature, Teu) was recorded only in a few inclusions in the range −28 to −46 °C (i.e. below the NaCl–H_2O and NaCl–KCl–H_2O eutectics), indicating the presence of $CaCl_2$ and/or $MgCl_2$ in addition to NaCl. No clear relationship is observed between Tmice and Teu. The final homogenisation, into the liquid state, occurred typically between 160 and 190 °C, but ranged from 140–240 °C (Fig. 6F).

Interpretation of fluid inclusion data

The textural and cross cutting relationships presented by the three populations of fluid inclusions, in addition to their microthermometric data, indicate that type 1 and 2 inclusions are the most precocious and that they resemble primary inclusions of Roedder (1984), whereas type 3 inclusions are clearly late secondary. Although it is difficult to preserve primary inclusions in a dynamic, developing quartz vein-fault system (McCuaig and Kerrich 1998), the absence of major deformation in the host quartz reinforces this primary character of the earlier type 1 and 2 fluid inclusions.

Although there is no clear spatial relationship linking any fluid inclusion assemblage to gold deposition, the primary character demonstrated by type 1 and 2 inclusions, the presence of gold particles in the host quartz and the absence of another event with temperature conditions higher than those recorded by these inclusion types indicate that these populations most likely represent the vein-forming hydrothermal fluids. Moreover,

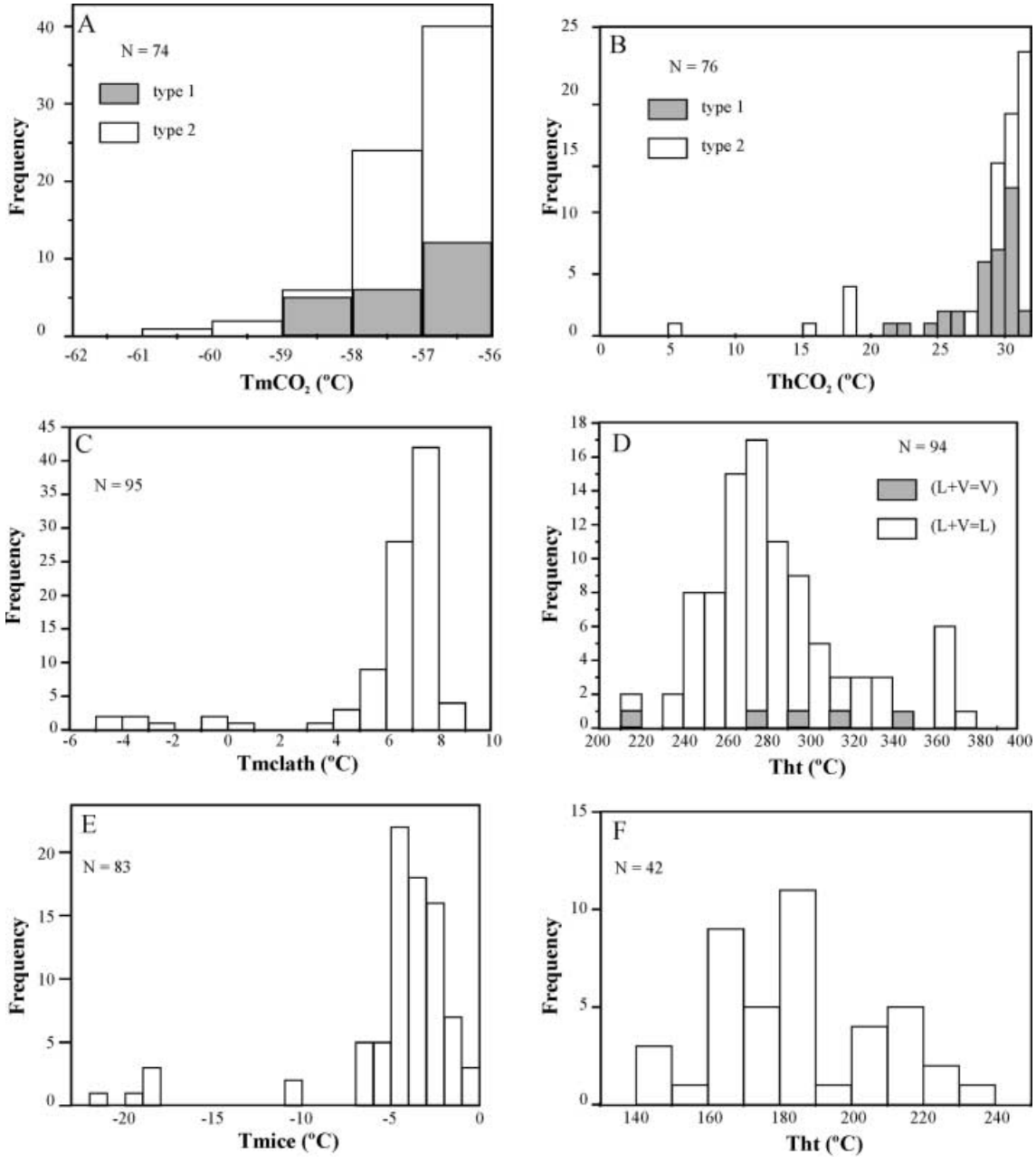

Fig. 6 Histograms showing **A–D** the microthermometric results for the CO_2-bearing types 1 and 2 and **E–F** aqueous type 3 fluid inclusions from the Guarim deposit

the petrographic and microthermometric similarities between the inclusions populations in the two textural types of quartz suggest that they are part of the same hydrothermal episode. They are, therefore, assumed to be related to gold deposition.

The inclusions show variability in CO_2:H_2O ratio in coexisting inclusions, relatively spread densities, and a wide range of final homogenisation temperatures. These are typical characteristics of the heterogeneous state, which could be caused by a variety of processes, such as mixing, unmixing and post-entrapment changes.

The H_2O–CO_2 fluids theoretically could have been produced by mixing of different proportions of fluids from type 1 and 3 inclusions (Pichavant et al. 1982; Anderson et al. 1992). However, petrographic and cross-cutting relationships, as well as microthermometry (Tht) have shown that the fluid in the type 3 inclusions was trapped late in the hydrothermal history of the Guarim quartz vein. Additionally, mixing of fluids requires correlation between Tht and salinity (Cathelineau and Marignac 1994; Pan and Fleet 1995), which is not the case here. The only evidence of mixing is the localised occurrence of high-salinity type 2 and 3 inclusions in a single cluster, which is interpreted as modification of the type 2 inclusions by the late infiltration of a lower temperature saline aqueous fluid.

Table 1 Composition of the carbonic phase in carbonic and aqueous-carbonic fluid inclusions of the Guarim gold mineralisation, estimated from Raman spectroscopy

Sample no.	Type	CO_2(%)	N_2(%)
G1-3A	2	92	8
G1-3C1	2	91	9
G1-3C2	2	97	3
G1-3D	1	99	1
G1-7B	2	99	1
G1-7C	2	97	3
G1-7D	2	100	tr
G1-10D1	2	100	tr
G1-10D2	2	96	4
G2-4B	2	97	3
G2-4C	2	98	2
G2-5F1	1	99	1
G2-5F2	2	93	7

Unmixing or heterogeneous trapping (phase separation or immiscibility) of a previously homogeneous fluid has been commonly described as an important process operating in lode-gold systems (Robert and Kelly 1987; McCuaig and Kerrich 1998). Ramboz et al. (1982) established criteria to investigate whether populations of mixed CO_2–H_2O–NaCl inclusions could have been derived from the unmixing of an originally homogeneous fluid. First, the inclusions suspected of unmixing (types 1 and 2) should be contemporaneous and cogenetic, which is texturally demonstrated at Guarim by their coexistence in the same clusters and microdomains. Secondly, fluids must be trapped in different and random proportions, which is also observed to some extent in the Guarim quartz vein. Thirdly, liquid-rich and vapour-rich inclusions should homogenise (or decrepitate) in the same temperature range, respectively to liquid and to vapour. Type 2 inclusions homogenised mostly to liquid and some water-poor inclusions could be observed homogenising to vapour, broadly in the same range of temperature (Fig. 6D). However, for type 1 inclusions, this is hampered by the difficulty in detecting small quantities of water (<10 vol%) in the inclusions, and thus in the observation of final of homogenisation. Furthermore, most inclusions of this type decrepitate before homogenisation. But, as these inclusions are vapour-rich, and as no shrinking of the CO_2 bubble during heating was observed, it may be supposed that they homogenise to the vapour state (Roedder 1984).

Another criterion favouring fluid immiscibility (Ramboz et al. 1982; Robert and Kelly 1987; Frantz et al. 1992) is the preferential fractionation of salts into the aqueous-rich phase during phase separation. Accordingly, water-rich inclusions should have higher salinities than water-poor inclusions. This is not the case at Guarim, where salinities show a relatively narrow range (Fig. 6C), irrespective of their phase ratio.

Post-entrapment changes and/or re-equilibration of inclusions during exhumation or deformation have been also invoked to explain homogenisation temperature, composition and density variability; discrepant behaviour of fluid inclusion populations in relation to experimental data; and inconsistencies between fluid properties and enclosing environmental conditions of vein formation (Klemd et al. 1996; Ridley and Hagemann 1999). Volume changes, stretching and leakage (natural or in laboratory) may occur because of overpressure and deformation (Bakker and Jansen 1991; Johnson and Hollister 1995). Different P–T paths followed by the inclusions after their formation may provoke textural re-equilibration and affect microthermometric properties (Vityk and Bodnar 1995).

Selective post-entrapment removal of water has also been reported as associated with the crystallisation of hydrous minerals or induced by deformation (Hall and Sterner 1993; Johnson and Hollister 1995). The extraction may occur either by simple leakage or by some kind of diffusional mechanism (Hall and Sterner 1993), such as pipe diffusion along dislocations, subgrain boundaries, and other structural defects. According to Hall and Sterner (1993), this mechanism would imply a raise in the salinity, which could be evidenced by a correlation between inclusion size and salinity. This would not be caused by simple leakage. As already outlined, no significant salinity variation was recognised at Guarim. Thus, if some water loss occurred, it would be related to simple leakage.

Preferential water loss may also occur due to the strong polarity of the H_2O molecule. The molecule wets the quartz surfaces and remains outside the advancing crystal front during quartz growth, which results in CO_2-rich inclusions (Crawford and Hollister 1986).

Huizenga and Touret (1999) suggested that comparisons between the CO_2:H_2O ratio and the density of the carbonic phase may provide an indication as to whether phase separation or selective water leakage has occurred. Accordingly, if aqueous-carbonic inclusions have been generated by phase separation (immiscibility), then the density of the carbonic phase in water-rich inclusions should be lower than in water-poor inclusions. The opposite would indicate selective leakage. At Guarim, no clear relationship could be observed between these properties. Most of the inclusions have similar densities ($ThCO_2$ between 29 and 31 °C) and display the full range of phase ratios. The few type 2 inclusions with higher densities, show an intermediate phase ratio (CO_2 bubble occupying 30–50 vol%). Thus, no conclusion can be drawn from this criterion.

Finally, the statistical and graphical behaviour of the final homogenisation of the type 2 fluid inclusions, with the histogram slightly skewed to the left (Fig. 6D), is compatible with fluids produced by phase separation (Touret 1994). Plastically deformed inclusions should display an unimodal histogram slightly skewed to the right, with a low standard deviation, and fluid inclusions deformed in a brittle manner should show positive correlation between size and density (Vityk and Bodnar 1998).

Summarising, vertical trends in Tht versus salinity plots, which are typical of necking-down and leakage

during heating, and cause scattering in Tht data (Shepherd et al. 1985), are not present here. Although attempts were made to avoid measurement of inclusions showing evidence of necking-down or leakage, a few such inclusions may be recognised (for example, the higher Tht values in Fig. 6D) in the data. No clear relationship could be observed between properties such as inclusion size, phase ratio, salinity and density of the carbonic phase. Selective water loss via some diffusional mechanism is unlikely to have occurred. The investigated quartz is dominantly strain-free, displaying only weak undulatory extinction and no other signs of deformation, which precludes any significant leakage induced by plastic deformation. Although post-entrapment changes could not be unequivocally ruled out, the above reasoning suggests that they should not have played a major role in defining the fluid properties at Guarim. Despite the salinity fractionation criteria for immiscibility, which was not fulfilled, the heterogeneous trapping of an unmixed CO_2–H_2O–NaCl parent fluid is probably the best explanation for the petrographic and microthermometric behaviour of the investigated fluid inclusion assemblages. The spread in final homogenisation temperatures and densities can be regarded to be the consequence of the entrapment of unmixed fluids under pressure fluctuations (see discussion below). Accordingly, the CO_2–H_2O (type 2) inclusions provide the best approximation of the P–T–X of the mineralising fluid. The CO_2 (type 1) inclusions may have resulted from vapour separation during the unmixing process (immiscibility).

Estimation of fluid composition and densities

Bulk composition, density constraints, and isochores calculations (see next session) were obtained from microthermometric and Raman data, using the MacFlincor program (Brown and Hagemann 1994). The equation of state of Bowers and Helgeson (1985) was used for type 2 inclusions, whereas the equation of state of Holloway (1981) was used for type 1 inclusions.

Microthermometric and laser Raman analyses have shown that CO_2 is the main constituent of the non-aqueous phase in type 1 and 2 inclusions. Semi-quantitative estimations, based on integration of peak areas of the Raman spectra (Table 1), support the presence of only traces to minor N_2. The low contents of N_2 have not affected the microthermometric properties of the fluid inclusions, such as Tmcla and $ThCO_2$, except by the minor lowering of $TmCO_2$. Thus, the calculated bulk composition of the fluid is XH_2O: 60–94 mol%; XCO_2: 3–35 mol% (typically 5–10 mol%); XNaCl: 1–3 mol%; and traces of N_2.

The density of the CO_2 phase (given by $ThCO_2$) ranges from 0.33–0.82 g/cm^3, although typically between 0.53 and 0.60 g/cm^3. Bulk densities are also relatively low to moderate, varying between 0.70 and 0.97 g/cm^3, with most of the values concentrating in the range 0.85–0.95 g/cm^3. Salinities of the aqueous phase of type 2 fluid inclusions, derived from Tmcla, vary typically between 3.9 and 7.5 wt% NaCl equiv., clustering at about 4.9 wt% NaCl equiv. In type 3 fluid inclusions, Tmice indicates salinities clustering between 2 and 6.5 wt% NaCl equiv.

Constraints on P–T

As phase separation (immiscibility) and simultaneous trapping have been proven, this means that the fluid inclusions were trapped on or near the solvus of the CO_2–H_2O–NaCl system and that their final homogenisation equals the true trapping temperature of the fluid, needing no correction for pressure. Accordingly, P–T of trapping could be determined by the intersection of the isochores of the end-members (Roedder and Bodnar 1980). However, the range of densities observed at Guarim does not allow calculation of isochores with different slopes that cross in a specific P–T space. Thus, instead of determining a single point in this space, an approach that determines boundary P–T conditions is preferred.

Given the lack of an independent geothermometer, the procedure adopted for limiting these conditions was one using the full range of the H_2O–CO_2 isochores (higher and least bulk densities) with the solvus for $XCO_2 = 10$ mol% and 6 wt% NaCl equiv. (Bowers and Helgeson 1983). This solvus has been chosen because it lies within the typical calculated XCO_2 interval and because it fits better with the temperature range obtained by the fluid inclusion study. Much higher and much lower values of XCO_2, would intersect the isochores in higher and lower values of temperature, respectively, than those recorded in the fluid inclusions. Using this approach, the P–T boundary conditions outlined for the Guarim deposit are 270–320 °C and 0.86–2.9 kb (Fig. 7). This temperature interval is broadly coincident with the range of Tht (one standard deviation).

As outlined above, the ranges of Tht, densities and compositions have likely been produced by phase separation and do not represent major post-entrapment changes in the fluid inclusions. These ranges represent the physico-chemical properties of the mineralising fluid, from which the host quartz has precipitated, and reflect variations during the mineralising process (Schmidt Mumm et al. 1997). Moreover, as the inclusions were trapped along an active fault system, and given that the local host rock temperature is unlikely to vary significantly during vein development (Robert et al. 1995), the spread in isochores and in the pressure data probably reflects pressure fluctuations during the hydrothermal event. In this case, according to Hagemann and Brown (1996), the mean of the pressure data likely represents average pressure conditions during the mineralising process ($\sim$1.5 kb at Guarim).

Pressure fluctuation is a common process described for many shear- and fault-hosted lode gold deposits (e.g. Robert and Kelly 1987; Cox et al. 1995). In such an

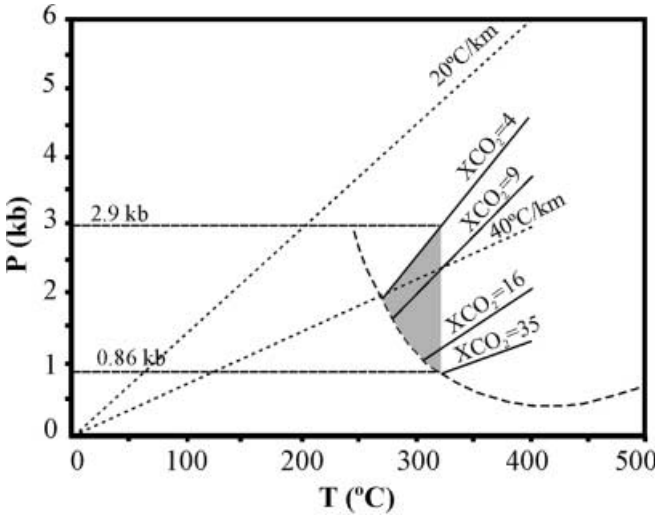

Fig. 7 Pressure–temperature diagram showing isochores covering the range of compositions and densities of aqueous-carbonic (type 2) inclusions (*solid lines* labelled *XCO_2*) from Guarim. The *shaded area* represents the P–T conditions estimated for gold mineralisation, given by the intersection of the isochores with the solvus (Bowers and Helgeson 1983) for $XCO_2 = 10$ and 6 wt% NaCl equiv. (*dashed curve*). The *dotted lines* show, for comparison, the range of thermal gradients that are commonly found in environments such as that of Guarim

active, structurally-controlled hydrothermal system, fluid pressure varies from hydrostatic to lithostatic conditions, and often exceeds lithostatic conditions (Sibson 1987). On the other hand, in strike–slip systems, where $\sigma 3$ is subhorizontal, the propagation of vertical extensional fractures breaks the pressure seals, allowing pressure to drop (Cox 1990). Accordingly, supralithostatic pressure regimes tend to be localised and short-lived (Sibson 1987; Cox 1990).

At Guarim, microstructures occurring as intra- and trans-granular fractures, the weak and localised undulose extinction of quartz, macroscopic features including buck massive and open space filling textures, the presence of extensional veinlets and hydrothermal breccias, and the occurrence of ductile fabric along one margin of the vein emplaced in a brittle environment, all coexist. These features indicate overpressurised fluids and alternation between brittle hydraulic fracturing and/or slip dislocation and localised ductile behaviour, respectively representing fast and low strain rates (Henderson and McCaig 1996; McCuaig and Kerrich 1998).

Constraints on f_{O_2}–f_{S_2}–pH

Thermodynamic parameters, such as oxygen and sulphur fugacities and pH, are important because they influence the mechanisms of gold transport and deposition. Oxygen fugacities were calculated for the full range of P–T–XCO_2 of the mineralising fluid, based on fluid inclusion data and assuming the $C + O_2 = CO_2$ equilibrium. The low N_2 content of the fluid does not influence the estimates and the volatile species may be considered as an inert component (Schwartz et al. 1992). Possible sources of uncertainties in the results may be caused by variations in pressure estimations and the salt content of the fluid. The latter, in the range displayed by the mineralising fluid, tends to enhance the CO_2 activity (Ramboz et al. 1985). Equations for f_{O_2} and log K are from Ohmoto and Kerrick (1977) and the fugacity coefficient is taken from Ryzhenko and Volkov (1971). The calculated values for log f_{O_2} range from −29.4 to −34.5, which fall between the HM and QMF solid buffers (Fig. 8), indicating relatively reduced conditions for the mineralising fluid. The presence of minor magnetite indicates that, at least transiently, the fluid reached f_{O_2} conditions higher than those recorded in the fluid inclusions, but still below the HM buffer.

Based on the calculated f_{O_2} and assuming the equilibrium pyrite–chlorite, f_{S_2} can be assessed from an activity–activity diagram (Fig. 9). Estimations made by this approach indicate log f_{S_2} of ∼−10 to −11, also suggesting a mildly reduced character for the fluid.

The pH was estimated from the salinity of the fluid (taken from the mode of the salinities of type 2 inclusions) and from mineral paragenesis. For a salinity range similar to that found at Guarim, Mikucki and Ridley (1993) calculated a near neutral pH ranging from 5.2–6.2. In addition, a near-neutral to slightly alkaline pH is indicated by the presence of carbonate (McQueen and Perkins 1995) and white mica (Romberger 1988) in the alteration assemblage.

Depth of vein emplacement

Vein textures and deposit-scale structures, as well as mineralogical and fluid inclusion evidence, are used to constrain the depth of vein emplacement. Vugs and

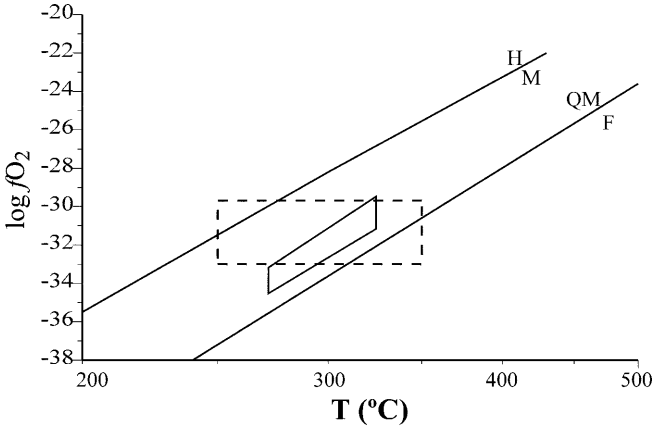

Fig. 8 T–f_{O_2} diagram showing the redox state of the gold-bearing solutions at Guarim (*heavy line*), obtained from the fluid inclusion study, and its relationships with the solid buffers quartz–magnetite–fayalite (*QMF*) and hematite-magnetite (*HM*) at 2 kb (Ohmoto and Kerrick 1977). The *dashed lines* limit the conditions for many studied Archaean lode-gold deposits (Groves and Foster 1991)

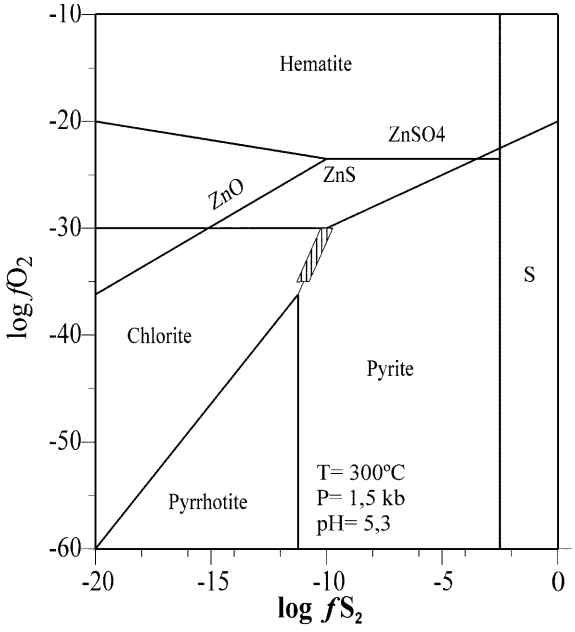

Fig. 9 Stability fields for selected mineral phases as a function of f_{O_2} and f_{S_2}, showing the redox state conditions for the mineralising fluid at Guarim. The f_{O_2} is obtained from fluid inclusion composition and f_{S_2} is given by coexisting pyrite–chlorite. Modified from Fayek and Kyser (1995, and references therein)

open-space filling textures have been considered as typical of shallowly-formed veins, but they may also occur at deep crustal levels either in compressional or in extensional regimes (Hodgson 1989; Cox et al. 1995). This suggests that fluid pressure has been equal to (Robert et al. 1995), or has exceeded, lithostatic conditions (Murphy and Roberts 1997), as the preservation of open spaces may be ascribed to low effective confining pressure (Hagemann et al. 1992).

Microscopic and macroscopic features suggest that vein emplacement has occurred in an active fault and that deformation was essentially brittle. Localised ductile shearing in the margin of the vein was likely produced by high fluid pressure (McCuaig and Kerrich 1998), which promoted fracture propagation and hydrothermal alteration with consequent chemical softening of the wallrock, allowing strain localisation and the development of the narrow ductile deformation zone (Segall and Simpson 1986; Gibson 1990; Tourigny and Tremblay 1997). The spatial association of the brittle and ductile structures, and their identical orientations and mineralogy (quartz, chlorite, white mica and carbonate), suggest that they are genetically related, and formed under similar stress conditions (Tourigny and Tremblay 1997) and metamorphic grade (greenschist). These mineralogical, textural and structural parameters provide evidence for the emplacement of the Guarim gold–quartz vein in lower epizonal to upper mesozonal crustal levels (i.e. ~4–7 km). Moreover, the bulk stress regime was brittle, with deformation conditions controlled by varying fluid pressure and fluid-rock ratios through time.

Depth estimates from pressure data obtained from fluid inclusion studies in lode-gold systems usually assume lithostatic conditions (Hagemann and Brown 1996). Accordingly, the full range of pressures determined at Guarim would imply a depth range from 4–10 km, but the deeper levels probably are not compatible with the textural and structural aspects discussed above. Thus, the more compelling textural and structural evidence are preferred here to constrain the depth of vein formation.

Structural and hydrothermal fluid evolution

Although the ultimate sources of the mineralising fluid at Guarim cannot be confidently determined, carbonate and sulphide enrichments around the vein are suggestive that the mineralising fluid was not in equilibrium with the host rock and must have been externally derived (Cox et al. 1995). From an integrated structural, mineralogical and fluid point of view, a valve/pump model is envisaged, following Sibson (1987), Cox et al. (1995) and Robert et al. (1995). Accordingly, externally derived and, possibly, deeply-sourced fluids ascended to a seismically active environment, through suitable pathways that are represented by the regional, subvertical strike-slip fault system. Under supralithostatic conditions, a network of hydraulic fractures developed in the host rock prior to a slip event, driving the fluid out of the fault and altering the adjacent wallrock. Immediately after rupture (slip), a pressure drop within the fault zone occurred, causing the fluid to migrate back into the fault. It is not clear, however, if this has taken place as a cyclic or single-pass process during the dynamic evolution of the Guarim fault. Gold and associated sulphides were introduced probably late in this structural-hydrothermal evolution, as suggested by the preservation of the open-space-filling textures and by the strain free behaviour of the quartz and pyrite grains.

The presence of sulphide minerals in the alteration zones suggests that H_2S (or HS^-) could have been an important component of the hydrothermal fluid. This assumption, together with the composition and homogenisation temperatures displayed by the fluid inclusions, the range in the thermodynamic parameters, and the low base metals contents of the alteration assemblage indicate that gold was transported as a reduced sulphur complex. For these conditions, $Au(HS)_2^-$ was probably the transporting complex (Benning and Seward 1996).

The destabilisation of the transporting complex caused deposition of gold from solution. At Guarim, this probably occurred by a combination of fluid-rock interaction and fluid immiscibility. Fluid-rock reactions are supported by the spatial association of gold and sulphides, in both the vein and altered wallrock, and by the potassium (assuming muscovite as the white mica) and CO_2 enrichments of the host rock. Sulphidation by reaction of sulphur in the ore fluid with Fe–Mg-bearing

minerals (biotite ± amphibole) of the host rock led to the S-complex breakdown and gold precipitation. The formation of white mica (K metasomatism) released H_2 to the fluid, while the carbonatisation of the host rock removed CO_2 from the fluid, both producing changes in the pH conditions. In addition, CO_2 was removed from the fluid during phase separation triggered by pressure fluctuations, raising both pH and f_{O_2} (Bowers 1991). Furthermore, the presence of gold and sulphides both in the vein and in the wallrock alteration zones suggests that redox reactions may have influenced gold precipitation (e.g. Cox et al. 1995). All these processes, which are typically considered as very effective for gold deposition (Shenberger and Barnes 1989), may have concurred at Guarim.

Concluding remarks

The gold metallogeny of the Tapajós province as a whole is far from well understood, as current models generally still lack detailed geological, geochemical and geochronological data. Robert (1996) suggested a group of shallowly-formed gold deposits in Tapajós that are similar to the intrusion-related gold deposits described by Sillitoe (1991), which are common in Cenozoic subduction-related environments. Coutinho et al. (1997) extended this model to define two types of gold deposits based on structural and petrological parameters: a younger group, defined by intrusion-related lodes, breccias, stockworks and disseminations, and an older group represented by quartz veins associated with regional-scale shear zones. Dreher et al. (1998) indicated epithermal conditions (adularia–sericite type) for, at least, two deposits (Davi and Joel). Although geochronological data are still scarce and preliminary, the available data point to at least two gold-forming events in the Tapajós province, occurring at 1.96 Ga (Vasquez et al. 2000) and 1.88 Ga (Santos et al. 1997). These two events are also suggested by Coutinho et al. (2000). The characteristics at Guarim fit best with those from quartz vein deposits of the older age.

Irrespective of the adopted model, the following aspects found at Guarim must be taken into account: (1) the dominantly brittle nature of the hosting structure; (2) the variable textures of the quartz, from massive to open space-filling; (3) the presence of hydrothermal breccias; (4) the alteration assemblage, composed of quartz–white mica–chlorite–carbonate–pyrite; (5) the fluid composition (low salinity, CO_2-rich) and (6) P–T–f_{O_2} conditions. The first three elements have been usually considered as pertaining to shallowly emplaced deposits (epithermal, porphyry, but, also, shallow mesothermal deposits) and the latter three situations are typical of mesothermal deposits.

The fluid characteristics encountered at Guarim are quite different from those found at the Joel and Davi epithermal deposits (Dreher et al. 1998). They are compositionally identical to those found at the plastically-deformed Patinhas quartz vein (Klein et al. 2000), which was emplaced in a similar setting, but probably at deeper crustal levels. These features (depth of formation, fluid composition, wallrock alteration) rule out both epithermal and porphyry-related deposit types. Similar textural and structural characteristics have been described for Australian lode-gold deposits at Wiluna (Hagemann et al. 1992) and Racetrack (Gebre-Mariam et al. 1993). Some Korean mesothermal deposits have similar characteristics as well (Shelton et al. 1988; So and Yun 1997), although in all examples controversy still surrounds the possible sources of the fluids.

Guarim shows many similarities with mesothermal deposits of Archaean to Cenozoic age (McCuaig and Kerrich 1998), or, following the proposals of Gebre-Mariam et al. (1995) and Groves et al. (1998), it can be classified as an epizonal to mesozonal orogenic gold deposit. A possible origin for the mineralising fluid, in part supported by the physico-chemical behaviour characterised in this work, may be deeply sourced fluids derived from the metamorphism of the basement rocks that have ascended to a brittle environment (McCuaig and Kerrich 1998). The mineralising episode is clearly post-metamorphic and post-deformational in relation to the host Cuiú-Cuiú Complex rocks. The characteristics are also permissive of late-stage magmatic fluids (Burrows and Spooner 1987; McCuaig and Kerrich 1998), which could be ascribed to the intrusion of the Creporizão granitoids.

Obviously, more data are necessary before sources for fluids and metals for Guarim and other gold deposits of the evolving and likely future economically important Tapajós province can be confidently identified. Nevertheless, the detailed study of Guarim allowed better development of a genetic model for this widespread deposit style.

Acknowledgements The authors thank Dr Raimundo Netuno N. Villas (UFPA) for providing access to the Fluid Inclusion Laboratory, where the microthermometric analyses were performed. Ruy B.C. Bahia and Marcos L.E.S. Quadros (CPRM) are acknowledge for field support and discussions on the geology of the Cuiú-Cuiú area, and Ana Maria Dreher (CPRM) is thanked for her comments on an earlier draft of this manuscript. We express our appreciation to the journal editor, Dr Richard Goldfarb, and to the reviewers, Drs Roberto P. Xavier and Reiner Klemd. Their criticisms and suggestions certainly improved the final version of this work.

References

Almeida ME, Brito MFL, Ferreira AL, Monteiro MAS, Popini MVF, Dreher AM (1998) Mineralizações auríferas associadas a vulcanismo ácido e intermediário na Folha Vila Mamãe Anã, Província Mineral do Tapajós. Congresso Brasileiro de Geologia, 40, Abstr vol, p 148

Almeida ME, Ferreira AL, Brito MFL de, Monteiro MAS (1999) Proposta de evolução tectono-estrutural para a região do médio-alto curso do rio Tapajós (Estados do Pará e Amazo-

nas). Simpósio de Geologia da Amazônia, 6, Extended Abstr vol, pp 297–300
Almeida ME, Brito MFL, Ferreira AL, Monteiro MAS (2000) Projeto Especial Província Mineral do Tapajós. Geologia e recursos minerais da Folha Vila Mamãe Anã (SB.21-V-D), Estados do Pará e Amazonas, escala 1: 250,000. Nota Explicativa. CPRM (on CD-ROM)
Anderson MR, Rankin AH, Spiro B (1992) Fluid mixing in the generation of mesothermal gold mineralization in the Transvaal Sequence, Transvaal, South Africa. Eur J Mineral 4: 933–948
Bahia RBC, Quadros MLES (2000) Geologia e recursos minerais da Folha Caracol (SB.21-X-C), Estado do Pará. Escala 1: 250,000. Nota Explicativa. CPRM (on CD-ROM)
Bakker RJ, Jansen BH (1991) Experimental post-entrapment water loss from synthetic CO_2–H_2O inclusions in natural quartz. Geochim Cosmochim Acta 55: 2215–2230
Benning LG, Seward TM (1996) Hydrosulphide complexing of Au(I) in hydrothermal solutions from 150–400 °C and 500–1500 bar. Geochim Cosmochim Acta 60: 1849–1871
Bowers TS (1991) The deposition of gold and other metals: pressure-induced fluid immiscibility and associated stable isotopes signatures. Geochim Cosmochim Acta 55: 2417–2434
Bowers TS, Helgeson HC (1983) Calculation of the thermodynamic and geochemical consequences of non-ideal mixing in the system H_2O–CO_2–NaCl on phase relations in geological systems: equation of state for H_2O–CO_2–NaCl fluids at high pressures and temperatures. Geochim Cosmochim Acta 47: 1247–1275
Bowers TS, Helgeson HC (1985) Fortran programs for generating fluid inclusion isochores and fugacity coefficients for the system H_2O–CO_2–NaCl at high pressures and temperatures. Comp Geosci 11: 203–213
Brown PE, Hagemann SG (1994) MacFlinCor: a computer program for fluid inclusion data reduction and manipulation. In: De Vivo B, Frezzotti ML (eds) Fluid inclusions in minerals: methods and applications. Virginia Tech, Blacksburg, pp 231–250
Burrows DR, Spooner ETC (1987) Generation of a magmatic H_2O–CO_2 fluid enriched in Mo, Au and W within an Archean sodic granodiorite stock, Mink Lake, northwestern Ontario. Econ Geol 82: 1931–1957
Cathelineau M, Marignac C (1994) Use of fluid inclusions for a better understanding of intracontinental geothermal activities. In: De Vivo B, Frezzotti ML (eds) Fluid inclusions in minerals: methods and applications. Virginia Tech, Blacksburg, pp 309–326
Cordani UG, Sato K (1999) Crustal evolution of the South American Platform, based on Sr and Nd systematics in granitoid rocks. 2nd South American symposium on isotope geology, Cordoba, Argentina. Serviço Geologico Minero Argentino, pp 525–528
Cordani UG, Brito Neves BB (1982) The geologic evolution of South America during the Archean and Early Proterozoic. Rev Brasil Geociênc 12: 78–88
Costa LTR, Carvalho JMA (1999) Tipologia de mineralizações auríferas da região sul da Província Tapajós – Pará. Simpósio de Geologia da Amazônia, 6, Extended Abstr vol, pp 176–179
Coutinho MGN, Liverton T, Souza EC de (1997) Granitic magmatism and related gold mineralization in Tapajós Mineral Province, Amazonian area, Brazil. In: Second International Symposium on Granites and associated Mineralizations, ISGAM II, Ext Abstr vol, pp 46–47
Coutinho MGN, Santos JOS, Fallick AE, Lafon JM (2000) Orogenic gold deposits in Tapajós Mineral Province, Amazon, Brazil. International Geological Congress, 31 (on CD-ROM)
Cox SF (1990) Fluid pressure regimes and fluid dynamics during deformation of low-grade metamorphic terranes – implications for the genesis of mesothermal gold deposits. NUNA research conference on greenstone gold and crustal evolution. Val D'Or, Quebec, Abstr vol, pp 30–32
Cox SF, Etheridge MA (1983) Crack-seal fibre growth mechanisms and their significance in the development of oriented layer silicate microstructures. Tectonophysics 92: 147–170
Cox SF, Sun SS, Etheridge MA, Wall VJ, Potter TF (1995) Structural and geochemical controls on the development of turbidite-hosted gold quartz vein deposits, Wattle Gully mine, Central Victoria, Australia. Econ Geol 90: 1722–1746
Crawford ML, Hollister LS (1986) Metamorphic fluids: the evidence from fluid inclusions. In: Walther JV, Wood BJ (eds) Fluid rock interaction during metamorphism. Physical geochemistry, vol 5. Springer, Berlin Heidelberg New York, pp 1–35
Dowling K, Morrison G (1989) Application of quartz textures to the classification of gold deposits using North Queensland examples. Econ Geol Monogr 6: 342–355
Dreher AM, Vlach S, Martini SL (1998) Adularia associated with epithermal gold veins in the Tapajós Mineral Province, Pará State, northern Brazil. Rev Brasil Geociênc 28: 397–404
Faraco MTL, Carvalho JMA, Klein EL (1997) Carta metalogenética da Província Aurífera do Tapajós. In: Costa ML da, Angélica RS (eds) Contribuições à geologia da Amazônia. FINEP/SBG, Belém, pp 423–437
Fayek M, Kyser TK (1995) Characteristics of auriferous and barren fluids associated with the Proterozoic Contact Lake lode gold deposit, Saskatchewan, Canada. Econ Geol 90: 385–406
Ferreira AL, Almeida ME, Brito MFL, Monteiro MAS (2000) Projeto Especial Província Mineral do Tapajós. Geologia e recursos minerais da Folha Jacareacanga (SB.21-Y-B), Estados do Pará e Amazonas, escala 1: 250,000. Nota Explicativa. CPRM (on CD-ROM)
Frantz JD, Popp RK, Hoering TC (1992) The compositional limits of fluid immiscibility in the system H_2O–NaCl–CO_2 as determined with the use of synthetic fluid inclusions in conjunction with mass spectrometry. Chem Geol 98: 237–255
Gebre-Mariam M, Groves DI, McNaughton NJ, Mikucki EJ, Vearncombe JR (1993) Archaean Au–Ag mineralisation at Racetrack, near Kalgoorlie, Western Australia – a high crustal-level expression of the Archaean composite lode-gold system. Mineral Deposita 28: 375–387
Gebre-Mariam M, Hagemann SG, Groves DI (1995) A classification scheme for epigenetic Archaean lode-gold deposits. Miner Deposita 30: 408–410
Gibson R (1990) Nucleation and growth of retrograde shear zones: an example from the Needle Mountains, Colorado, USA. J Struct Geol 12: 339–350
Groves DI, Foster RP (1991) Archaean lode-gold deposits. In: Foster RP (ed) Gold metallogeny and exploration. Blackie, Glasgow, pp 63–103
Groves DI, Goldfarb RJ, Gebre-Mariam M, Hagemann SG, Robert F (1998) Orogenic gold deposits: a proposed classification in the context of their crustal distribution and relationship to other gold deposit types. Ore Geol Rev 13: 7–27
Hagemann SG, Brown PE (1996) Geobarometry in Archean lode-gold deposits. Eur J Mineral 8: 937–960
Hagemann SG, Groves DI, Ridley JR, Vearncombe JR (1992) The Archean lode gold deposits at Wiluna, Western Australia: high-level brittle-style mineralization in a strike-slip regime. Econ Geol 87: 1022–1053
Hall DL, Sterner SM (1993) Preferential water loss from synthetic fluid inclusions. Contrib Mineral Petrol 114: 489–500
Henderson IHC, McCaig AM (1996) Fluid pressure and salinity variations in shear zone-related veins, Central Pyrenees, France: implications for the fault-valve model. Tectonophysics 262: 321–348
Hodgson CJ (1989) The structure of shear-related, vein-type gold deposits: a review. Ore Geol Rev 4: 231–273
Holloway JR (1981) Composition and volumes of supercritical fluids in the Earth crust. In: Hollister LS, Crawford ML (eds) Fluid inclusions: applications to petrology, vol 6. Short course handbook. Mineralogical Association of Canada, Calgary, pp 13–38
Huizenga JM, Touret JLR (1999) Fluid inclusions in shear zones, the case of the Umwindsi shear zone in the Harare–Shamva–Bindura greenstone belt, NE Zimbabwe. Eur J Mineral 11: 1079–1090

Jébrak M (1997) Hydrothermal breccias in vein-type ore deposits: a review of mechanisms, morphology and size distribution. Ore Geol Rev 12: 111–134

Johnson EL, Hollister LS (1995) Syndeformational fluid trapping in quartz: determining the pressure–temperature conditions of deformation from fluid inclusions and the formation of pure CO_2 fluid inclusions during grain-boundary migration. J Metamorph Geol 13: 239–249

Klein EL, Vasquez ML (2000) Projeto Especial Província Mineral do Tapajós. Geologia e recursos minerais da Folha Vila Riozinho (SB.21-Z-A), Estado do Pará, escala 1: 250,000. Nota Explicativa. CPRM (on CD-ROM)

Klein EL, Vasquez ML, Santos A, Martins RC (1997) Structural elements of the Maloquinha Intrusive Suite in Tapajós Mineral Province, northern Brazil, and the emplacement of the plutons. Second International Symposium on Granites and Associated Mineralizations, ISGAM II, Extended Abstr vol, pp 313–314

Klein EL, Vasquez ML, Santos A, Costa LTR (1999) Geologia e controle estrutural das mineralizações auríferas na Folha Vila Riozinho e NW da Folha Rio Novo, Província Tapajós. Simpósio de Geologia da Amazônia, 6, Extended Abstr vol, pp 128–131

Klein EL, Costa LTR, Carvalho JMA (2000) Fluid inclusion studies at the Patinhas gold-quartz mineralisation, Tapajós Gold Province, Amazon, Brazil. Int Geol Congr 31 (on CD-ROM)

Klemd R, Hünken U, Olesch M (1996) Fluid composition and source of Early Proterozoic lode gold deposits of the Birimian volcanic belt, West Africa. Int Geol Rev 38: 22–32

McCuaig TC, Kerrich R (1998) P–T–t-deformation-fluid characteristics of lode gold deposits: evidence from alteration systematics. Ore Geol Rev 12: 381–453

McQueen KG, Perkins C (1995) The nature and origin of a granitoid-related gold deposit at Dargue's Reef, Major's Creek, New South Wales. Econ Geol 90: 1646–1662

Mikucki EJ, Ridley JR (1993) The hydrothermal fluid of Archaean lode-gold deposits at different metamorphic grades: compositional constraints from ore and wallrock alteration assemblages. Mineral Deposita 28: 469–481

Murphy PJ, Roberts S (1997) Evolution of a metamorphic fluid and its role in lode gold mineralisation in the Central Iberian Zone. Mineral Deposita 32: 459–474

Ohmoto H, Kerrick D (1977) Devolatilization equilibria in graphitic systems. Am J Sci 277: 1013–1044

Pan Y, Fleet ME (1995) The late Archean Hemlo gold deposit, Ontario, Canada: a review and synthesis. Ore Geol Rev 9: 455–488

Pichavant M, Ramboz C, Weisbrod A (1982) Fluid immiscibility in natural processes: use and misuse of fluid inclusion data. I. Phase equilibria analyses – a theoretical and geometrical approach. Chem Geol 37: 1–27

Quadros MLES, Bahia RBC, Klein EL, Vasquez ML, Almeida ME, Ricci PSF, Monteiro MAS (1999) As intrusões básicas da Província Mineral do Tapajós (PMT) e possibilidades de mineralizações associadas. Simpósio de Geologia da Amazônia, 6, Extended Abstr vol, pp 566–569

Ramboz C, Pichavant M, Weisbrod A (1982) Fluid immiscibility in natural processes: use and misuse of fluid inclusion data. II. Interpretation of fluid inclusion data in terms of immiscibility. Chem Geol 37: 29–48

Ramboz C, Schnapper D, Dubessy J (1985) The P–V–T–X–fO_2 evolution of H_2O–CO_2–CH_4-bearing fluid in a wolframite vein: reconstruction from fluid inclusion studies. Geochim Cosmochim Acta 49: 205–219

Ricci PSF, Vasquez ML, Santos A, Klein EL, Jorge João X, Martins RC (1999) Suíte Intrusiva Creporizão – Província Tapajós: proposta e critérios de definição. Simpósio de Geologia da Amazônia, 6, Extended Abstr vol, pp 519–522

Ridley J, Hagemann SG (1999) Interpretation of post-entrapment fluid-inclusion re-equilibration at the Three Mile Hill, Marvel Loch and Griffins Find high-temperature lode-gold deposits, Yilgarn Craton, Western Australia. Chem Geol 154: 257–278

Robert F (1996) Tapajós Gold Project, Pará State, Brazil. Mission Report, CIDA, Project 204/13886, Canada–Brazil cooperation project for sustainable development in the mineral sector. GSC, Ottawa

Robert F, Kelly WC (1987) Ore-forming fluids in Archean gold-bearing quartz veins at the Sigma Mine, Abitibi greenstone belt, Quebec, Canada. Econ Geol 82: 1464–1482

Robert F, Boullier AM, Firdaous K (1995) Gold-quartz veins in metamorphic terranes and their bearing on the role of fluids in faulting. J Geophys Res 100(B7): 12861–12879

Roedder E (1984) Fluid inclusions. Rev Mineral, Mineral Soc Am, vol 12

Roedder E, Bodnar RJ (1980) Geologic pressure determinations from fluid inclusion studies. Annu Rev Earth Planet Sci 8: 263–301

Romberger SB (1988) Geochemistry of gold in hydrothermal deposits. US Geol Surv Bull 1857-A: A9–A25

Ryzhenko BN, Volkov VP (1971) Fugacity coefficients of some gases in a broad range of temperature and pressures. Geochim Int 8: 468–481

Santos JOS, Hartmann LA, Gaudette HE (1997) Reconnaissance U–Pb in zircon, Pb–Pb in sulfides and review of Rb–Sr geochronology in the Tapajós Gold Province Pará/Amazonas states, Brazil. South American Symposium on Isotope Geology, 1, Extended Abstr vol, pp 280–282

Santos JOS, Hartmann LA, Gaudette HE, Groves DI, McNaughton NJ, Fletcher IR (2000) A new understanding of the provinces of the Amazon Craton based on integration of field mapping and U–Pb and Sm–Nd geochronology. Gondwana Res 3(4): 453–488

Santos RA (1998) Contribuição à análise estrututural dos jazimentos auríferos da região do Cuiú-Cuiú, Pará. CPRM

Santos RA (1999) Controle estrutural das mineralizações de ouro da Província Mineral do Tapajós. CPRM

Schmidt Mumm A, Oberthür T, Vetter U, Blenkinsop TG (1997) High CO_2 content of fluid inclusions in gold mineralisations in the Ashanti Belt, Ghana: a new category of ore forming fluids? Mineral Deposita 32: 107–118

Schwartz MO, Oberthür T, Amanor J, Gyapong WA (1992) Fluid inclusion re-equilibration and P–T–X constraints on fluid evolution in the Ashanti gold deposits, Ghana. Eur J Mineral 4: 1017–1033

Segall P, Simpson C (1986) Nucleation of ductile shear zones on dilatant fractures. Geology 14: 56–59

Shelton KL, So CS, Chang JS (1988) Gold-rich mesothermal vein deposits of the Republic of Korea: geochemical studies of the Jungwon gold area. Econ Geol 83: 1221–1237

Shenberger DM, Barnes HL (1989) Solubility of gold in aqueous sulfide solutions from 150 to 350 °C. Geochim Cosmochim Acta 53: 269–278.

Shepherd TJ, Rankin AH, Alderton DH (1985) A practical guide to fluid inclusion studies. Blackie, Glasgow

Sibson RH (1987) Earthquake rupturing as mineralizing agent in hydrothermal systems. Geology 15: 701–704

Sillitoe RH (1991) Intrusion-related gold deposits. In: Foster RP (ed) Gold metallogeny and exploration. Blackie, Glasgow, pp 165–209

So CS, Yun ST (1997) Jurassic mesothermal gold mineralisation of the Samhwanghak mine, Youngdong area, Republic of Korea: constraints on the hydrothermal fluid geochemistry. Econ Geol 92: 60–80

Tassinari CCG, Macambira MJB (1999) Geochronological provinces of the Amazonian Craton. Episodes 22: 174–182

Tassinari CCG, Cordani UG, Nutman AP, Van Schmus WR, Bettencourt JS, Taylor PN (1996) Geochronological systematics on basement rocks from Rio Negro-Juruena Province (Amazonian Craton) and tectonic implications. Int Geol Rev 38: 161–175

Teixeira W, Tassinari CCG, Cordani UG, Kawashita K (1989) A review of the geochronology of the Amazonian Craton: tectonic implications. Precambrian Res 42: 213–227

Touret JLR (1994) Fluid inclusions in sedimentary and diagenetic environments. In: De Vivo B, Frezzotti ML (eds) Fluid inclu-

sions in minerals: methods and applications. Virginia Tech, Blacksburg, pp 251–269

Tourigny G, Tremblay A (1997) Origin and incremental evolution of brittle/ductile shear zones in granitic rocks: natural examples from the southern Abitibi Belt, Canada. J Struct Geol 19: 15–27

Vasquez ML, Klein EL (2000) Projeto especial Província Mineral do Tapajós. Geologia e recursos minerais da Folha Rio Novo (SB.21-Z-C), Estado do Pará, escala 1: 250,000. Nota Explicativa. CPRM (on CD-ROM)

Vasquez ML, Klein EL, Quadros MLES, Bahia RBC, Santos A, Ricci PSF, Sachett CR, Silva CMG, Macambira MJB (1999) Magmatismo Uatumã na Província Tapajós – novos dados geocronológicos. Simpósio de Geologia da Amazônia, 6, Extended Abstr vol, pp 471–474

Vasquez ML, Klein EL, Macambira MJB, Santos A, Bahia RBC, Ricci PSF, Quadros MLES (2000) Geochronology of granitoids, mafic intrusions and mineralizations of the Tapajós Gold Province – Amazonian craton – Brazil. International Geological Congress, 31 (on CD-ROM)

Vearncombe JR (1993) Quartz vein morphology and implications for formation depth and classification of Archaean gold-vein deposits. Ore Geol Rev 8: 407–424

Vityk MO, Bodnar RJ (1995) Textural evolution of fluid inclusions in quartz during reequilibration, with applications to tectonic reconstruction. Contrib Mineral Petrol 121: 309–323

Vityk MO, Bodnar RJ (1998) Statistical microthermometry of synthetic fluid inclusions in quartz during decompression reequilibration. Contrib Mineral Petrol 132: 149–162